Elastic mismatch induced reduction of the thermal conductivity of silicon with aluminum nano-inclusions

Brian F. Donovan, Wade A. Jensen, Long Chen, Ashutosh Giri, S. Joseph Poon, Jerrold A. Floro, and Patrick E. Hopkins

CrossMark

Elastic mismatch induced reduction of the thermal conductivity of silicon with aluminum nano-inclusions

Brian F. Donovan,[1,a)] Wade A. Jensen,[2] Long Chen,[3] Ashutosh Giri,[4] S. Joseph Poon,[3] Jerrold A. Floro,[2] and Patrick E. Hopkins[2,3,4]

[1]Department of Physics, United States Naval Academy, Annapolis, Maryland 21402, USA
[2]Department of Materials Science and Engineering, University of Virginia, Charlottesville, Virginia 22904, USA
[3]Department of Physics, University of Virginia, Charlottesville, Virginia 22904, USA
[4]Department of Mechanical and Aerospace Engineering, University of Virginia, Charlottesville, Virginia 22904, USA

We use aluminum nano-inclusions in silicon to demonstrate the dominance of elastic modulus mismatch induced scattering in phonon transport. We use time domain thermoreflectance to measure the thermal conductivity of thin films of silicon co-deposited with aluminum via molecular beam epitaxy resulting in a Si film with 10% clustered Al inclusions with nanoscale dimensions and a reduction in thermal conductivity of over an order of magnitude. We compare these results with well-known models in order to demonstrate that the reduction in the thermal transport is driven by elastic mismatch effects induced by aluminum in the system. *Published by AIP Publishing.*
https://doi.org/10.1063/1.5019269

A fundamental understanding of the transport and interactions among the carriers of energy in composite solids is critical to applications ranging from computing, to jet engine performance, to waste heat recovery.[1–3] Thus, intricate knowledge of thermal scattering mechanisms can be used to design and engineer the thermal transport properties of solids. Of particular interest is the introduction of interfaces, impurities, and other crystalline defects to manipulate phonon transport in nanosystems. These features have offered dynamic flexibility in prescribing the thermal conductivity of solids via targeting specific phonon scattering processes. As a classic example, the theoretical formalism governing the scattering of phonons with mass impurities[4] has been rigorously experimentally vetted over the past half-century.[5–8] From this, novel functional nanomaterials have been designed with tailored thermal conductivities driven, in part, by this phonon mass-impurity interaction.[9–15] Figure 1 illustrates the degree of tunability that has been achieved using mass-impurity scattering in the silicon-germanium system. Addition of germanium to the silicon crystal results in significant reductions in the thermal conductivity ranging from a factor of four at Ge concentrations below 1 at. % (Ref. 6) to over an order of magnitude with high Ge concentrations and even lower with structuring into superlattices[16] and nanostructured superlattices to obtain thermal conductivities below the minimum limit of thermal conductivity.[17]

Clearly, the implications of phonon-mass impurity scattering on the thermal conductivity of solids have been well studied. However, systematic experimental studies that effectively focus on phonon scattering with other types of lattice imperfections are lacking in comparison. To systematically study the role of these imperfections in phonon transport, we must judiciously choose material systems in which the majority of phonon scattering would be

influenced by only one type of lattice imperfection (e.g., elastic modulus mismatch or mass difference). This is the case for the silicon germanium alloys in Fig. 1, where the elastic modulus and impurity volume mismatches between silicon and germanium effectively cancel each other out, leaving the differences in masses between silicon and
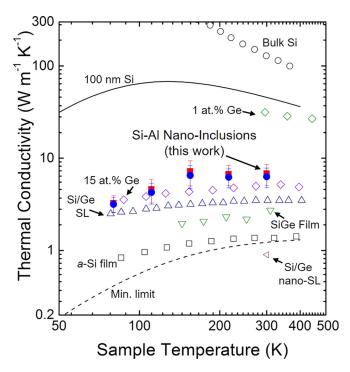

FIG. 1. Thermal conductivity of bulk single crystalline silicon (open circles)[18] and thin film amorphous silicon (open squares)[19] as well as models for 100 nm thick films (solid line) and the minimum limit to the thermal conductivity of silicon (dashed line). Also included is the thermal conductivity of Si-Ge alloys (diamonds),[6] a superlattice (upright triangles),[16] a 202 nm film (inverted triangles),[7] and a nano-structured superlattice (leftward triangle).[17] Additionally shown is the Si-Al thin film thermal conductivity measured in this work (filled circles and squares).

a)Electronic mail: bdonovan@usna.edu

germanium as the primary phonon scattering mechanism.[5,6] Using this approach enables us to evaluate common models for phonon scattering, particularly with respect to nanostructures,[9,20–22] and comment on the physical insight gained by phonon scattering theories as compared to measured data.

In this work, we aim to demonstrate effective scattering of phonons using imperfections that exhibit a large elastic mismatch, but have similar masses. The material system we have chosen to demonstrate this consists of nanoscale inclusions of aluminum in a silicon host, as there exists a considerable wealth of literature regarding thermal transport in silicon.[23–30] The aluminum-in-silicon material system offers a unique set of variables with respect to phonon scattering. The masses of Al and Si are very close at $26.98 \, \text{g mol}^{-1}$ and $28.09 \, \text{g mol}^{-1}$, respectively.[31] From this, we would expect models of phonon scattering based on a change in mass to predict a modest reduction in the thermal conductivity, not capturing the data that we have observed in this system. Models that take into account elastic mismatch, however, are based on the lattice parameter and the bond strength. These values vary quite significantly between Al and Si relative to the mass differences, with lattice parameters of $4.05 \, \text{Å}$ and $5.43 \, \text{Å}$ (Ref. 32) and elastic moduli of $76.2 \, \text{GPa}$ (Ref. 33) and $97.8 \, \text{GPa}$ (Ref. 34), respectively. This difference leads us to hypothesize that the elastic modulus mismatch between Al and Si can lead to reductions in the thermal conductivity of Al-Si-based material composites.

We evaluate this hypothesis based on known models for phonon scattering on the thermal conductivity of two-component composites that should capture a variety of physical mechanisms including nanoparticle scattering,[9] nanoparticle-host boundary scattering,[22] mass impurity scattering,[4] total diffuse scattering,[35] and scattering by elastic mismatch.[8] Through this evaluation, we show that elastic mismatch effects in Si, driven by the Al inclusions, are responsible for a reduction in the thermal conductivity of over an order of magnitude compared to bulk Si and Si thin films with similar thicknesses as those studied in this work.

In order to understand the origin of this reduction and various phonon scattering mechanisms contributing to this reduction in more detail, we measure the thermal conductivity of silicon films with Al nano-inclusions ("Si-Al films") over temperatures ranging from 80 K to 295 K. As shown in Fig. 1, we see that the trend of thermal conductivity with temperature is similar to that of the alloy, the superlattice, and amorphous films, which increases with increasing temperature (similar to the phononic heat capacity). This implies that anharmonic scattering of phonons (e.g., Normal and Umklapp) in the Si matrix of this Si-Al film do not offer limiting resistances to heat flow. In order to put these values in context, Fig. 1 also includes models for an intrinsic Si thin film and for the minimum limit to thermal conductivity, where we assume that the mean free path of phonons in the system is limited to a length scale corresponding to one half of a period of oscillation of each vibrational mode.

The Si-Al films were co-deposited in an ultra-high vacuum (UHV) hyperthermal molecular beam epitaxy (MBE) system with a routine base pressure of 1×10^{-10} Torr. The substrate was a 2-in. diameter undoped Si (001) wafer with a

miscut of $0.1°$. The wafers were cleaned using a multi-step chemical etching process to remove both organic and metallic contaminants. The final etching step creates a thick, passivating SiO_x layer. The passivated wafers were rinsed, dried, then fixed on a molybdenum sample holder and transferred through a load-lock chamber into the growth chamber. The protective SiO_x layer was desorbed *in situ* at $800°C$ for 10 min after a 15 h. prebake at $600°C$. The Si (001) 2×1 surface structure was monitored *in situ* using reflection high-energy electron diffraction (RHEED). The overall cleaning and buffer growth process produces a flat, atomically clean Si surface for epitaxial growth. Films were deposited by co-sputtering using variable-distance magnetron sputter guns as Si and Al sources. The working gas was 6 mTorr of getter- and liquid-nitrogen-purified argon. Prior to alloy growth, a 50 nm thick Si buffer layer was grown at $750°C$. Deposition rates for Si and Al were calibrated against a quartz crystal rate monitor in the substrate position. The films with compositions of $Si_{0.9}Al_{0.1}$ were grown at $250°C$, with a 100 nm thickness, at a total rate of about $0.2 \, \text{nm s}^{-1}$. Films were annealed at $250°C$ for 1.5 h and compared to the unannealed samples.

The surface-projected structure of the unannealed Si-Al film was examined using atomic force microscopy and scanning electron microscopy (SEM), which yielded similar results. In Fig. 2(a), we observe a heterogeneous structure with prominent inclusions. Energy dispersive spectroscopy (EDS) confirms that the inclusions are composed of Al, but cannot completely exclude minor alloying with Si. However, the mutual solubility of Al and Si is extremely low at the growth temperature of $250°C$.[36] The effective diameter of Al inclusions has lateral diameters of 136 ± 42 nm in the unannealed films and 157 ± 53 nm in the annealed films.

The technique used to measure the thermal conductivity of the Si-Al thin films is time domain thermoreflectance (TDTR). TDTR is an optical pump-probe measurement technique ideal for measuring the thermal properties of thin films.[37–39] An amplitude modulated pump creates a periodic heating event and the probe is time delayed in order to monitor the decay in the temperature of the sample surface at the pump frequency. This decay is fit to a thermal model for a multilayer system consisting of an Al thin film TDTR transducer, a 100 nm layer of the Si-Al film, and a Si substrate. Note that no additional processing was carried out to remove the native oxides on the surface of the Si-Al film prior to Al transducer evaporation. An in-depth description of the modeling of the TDTR data in this study, along with the sources of error for our data, can be found in the supplementary material. The results of thermal testing indicate that the room temperature thermal conductivity of the 100 nm Si-Al film is $6.8 \pm 0.3 \, \text{W m}^{-1}\text{K}^{-1}$ for the unannealed films and $6.0 \pm 0.3 \, \text{W m}^{-1}\text{K}^{-1}$ for the annealed films. This is a $10 \times$ reduction compared to the literature values of $\sim 60 \, \text{W m}^{-1}\text{K}^{-1}$ for Si thin films with similar thicknesses[30] (c.f. Fig. 1).

We model the lattice thermal conductivity of the Si-Al film, κ, according to the Callaway Model[40] involving the product of the volumetric heat capacity, C, the square of the phonon group velocity, v^2, and the phonon scattering time, τ. The product of these components is integrated over the
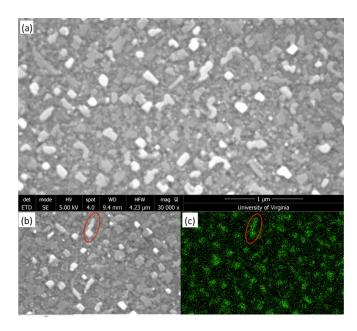
FIG. 2. (a) Plane-view scanning electron micrograph using secondary electrons of the unannealed Si-Al film along with the corresponding secondary electron image (b) and EDS Al maps (c). Example of identical features in both images are highlighted.
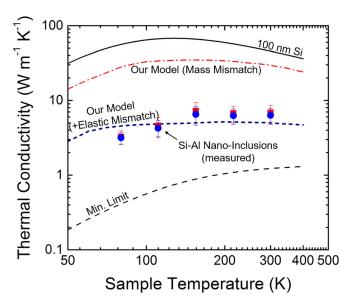

FIG. 3. Measured thermal conductivity over temperature of Si-Al films, seen as blue circles (unannealed) or red squares (annealed). Also included are accompanying models demonstrating the role of elastic mismatch in the significant reduction of the thermal conductivity.

phonon frequency, ω, for each branch of the phonon dispersion. We model the phonon dispersion of Si using a sine-type fit to literature data.[41]

In our formulation of this model, we determine τ via Matthiesen's rule

$$\tau^{-1} = AT\omega^2 \exp\left(\frac{-B}{T}\right) + D\omega^4 + \frac{v}{d} + \tau_{Al}^{-1}, \quad (1)$$

where T is the sample temperature and A, B, and D are fitting parameters based on data for the lattice thermal conductivity of bulk silicon or aluminum[42,43] to account for anharmonic phonon-phonon scattering in both Si and Al, and, in the case of Si, intrinsic impurity scattering. In the case of the model for the thermal conductivity of 100 nm thin film Si, d is the film thickness. Note that we do not include the intrinsic impurity scattering term in Al since the coefficients were determined with data from molecular dynamics simulations.[43] The thermal conductivity of the Al-inclusion-free host thin film of silicon is taken as the upper bound of our system, seen in Fig. 3. The lower bound to the thermal conductivity of the thin Si film is given by setting d equal to the lattice constant.[35]

The thermal conductivity of the host is determined taking into account phonon scattering from baseline effects such as phonon-phonon scattering, phonon-impurity scattering, and phonon-boundary scattering. This model takes into account the phonon scattering by the aluminum nanoparticles via the addition of the scattering time, τ_{Al} in Eq. (1). This scattering time follows the formulation by Mingo et al.,[9] who handled the phonon-nanoparticle scattering by accounting for cross-sectional scattering of long and short wavelength phonons separately. The short wavelength phonon scattering is dictated by the nanoparticle cross-section, σ_{Geo}, whereas the long wavelength phonons are scattered by

the Rayleigh mechanism, σ_{Ray}, that takes into account differences in densities between the nanoparticle and the host, given by

$$\sigma_{Geo} = 2\pi r^2 \left(1 - \frac{\sin\left(2\chi\left(\frac{q'}{q}-1\right)\right)}{\chi\left(\frac{q'}{q}-1\right)} + \frac{\left(\sin\left(2\chi\left(\frac{q'}{q}-1\right)\right)\right)^2}{\left(\chi\left(\frac{q'}{q}-1\right)\right)^2}\right), \quad (2)$$

$$\sigma_{Ray} = 2\pi^2 r^2 \chi^4 \left[\frac{\beta^2}{4}\left(\frac{M_{host}-M_{def}}{M_{host}}\right)^2\right] \times \frac{\cos(4\chi) + 4\chi\sin(4\chi) + 32\chi^4 - 8\chi^2 - 1}{16\chi^6}, \quad (3)$$

where r is the radius of the spherical nanoparticle, χ is the size parameter, defined as $\chi = qr$, where q is the incoming wave vector, q', is the scattered wave vector, δ is the volume size, and β is the polar angle. This relationship described the perturbation from differences in mass between the host and the nanoparticle, where M_{host} and M_{def} are the atomic mass of the host and the atomic mass of the nanoparticle, respectively. Using this mass difference, we calculate the thermal conductivity over temperature to compare with the data measured and the limits of the model for thermal conductivity of the thin film system, discussed previously. This mass difference model, shown also in Fig. 3, severely under-predicts the reduction in thermal conductivity from aluminum nano-inclusions (i.e., the model results over-predict the measured data). This under-prediction of the nano-inclusion scattering rate highlights the need to take into account other scattering mechanisms when considering the aluminum nano-inclusions in a silicon host.

Accordingly, we take into account the addition of elastic mismatch effects in the phonon scattering by modifying the high frequency (Rayleigh-like) scattering cross-section to include perturbation of atomic force constants. Thus, the part of Eq. (3) in square brackets is updated to include the addition of the following term

$$3\beta^8 \left(\frac{K_{host} - K_{def}}{K_{host}}\right)^2 \left(\frac{\sin(\beta q\delta/2)}{\beta q\delta/2}\right)^4, \qquad (4)$$

where K_{host} and K_{def} denote the force constant of the host medium and the force constant of the nanoparticle. This term is constructed similarly to the scattering strength from the mass difference; by perturbation to the Hamiltonian that describes the atoms and bonds as a spring-mass system. The formulation of these scattering strength terms is described in detail by Kim *et al.*,[21] where the scattering coefficient is dictated by either changes in the mass of the atoms or changes in the force constants binding the atoms together.

The result of including these elastic mismatch effects, seen in Fig. 3, is a model for the thermal conductivity of the aluminum nanoparticle in a silicon thin film that captures the significant reduction of their measured thermal conductivities compared to Si films. This distinct improvement in the agreement between the data and the elastic-mismatch-based scattering model suggests that the major mechanism behind the reduction in the thermal conductivity of Si when including ∼10% Al inclusions is largely based on differences in elastic moduli between the nanoparticle and the host.

There are a variety of assumptions that could lead to deviation from the measured data, particularly at low temperatures. This model assumes a very low level of impurities in the host material and discrete, spherical, uniform nanoparticles. In the real system, there is variation of nanoparticle size and shape, possible mixing between aluminum and the host silicon, and a variety of other non-idealities that will further impact the true thermal conductivity of the film. At low temperatures, boundary and impurity scattering can play a significant role in thermal transport limitation since anharmonic phonon scattering rates decrease. Furthermore, these models assume phonon-dominated thermal conductivity and thermal boundary conductance. Possibly, significant sources of thermal transport that are not accounted for in this treatment include phonon-electron coupling leading to significant electron thermal conductivity in aluminum nano-inclusions as well as electron-phonon thermal boundary resistance.[44] This electron-phonon thermal boundary resistance, R_{ep}, can be estimated via $R_{ep} = 1/\sqrt{G\kappa_p}$, where G is the electron-phonon coupling in aluminum [2.45×10^{17} W m^{-3}K^{-1} (Ref. [45])] and κ_p is the phonon thermal conductivity in Al. At room temperature, this electron-phonon thermal resistance is estimated to be ∼8 × 10^{-10} m^2 K W^{-1}. This thermal resistance is significant, but compared to the thermal resistance of the film itself (∼1.7 × 10^{-8} m^2 K W^{-1}), we see less than a 5% possible contribution from this mechanism, which is within the error of our measurement and could not be confidently resolved. Furthermore, other experimental work in systems similar to this aimed at specifically identifying the electron-phonon coupling at metal/non-metal interfaces have shown this mechanism to have a minor impact on thermal transport.[46–49]

In conclusion, we have used a combination of well-known models for thermal conductivity to evaluate the physical dynamics behind severely reduced thermal conductivity of thin Si films with nanoscale Al inclusions. We find that the model which best describes the data stems from a formulation that takes into account changes in atomic force constants as phonons move between the host and nano-inclusions. These findings lead to the conclusion that the major mechanism driving the observed reduction in the thermal conductivity of these films arises from an elastic mismatch between the host Si and the Al nano-inclusions. This clearly demonstrates the importance of considering elastic moduli differences in thermal transport through non-homogeneous materials. This will help guide the selection and engineering of materials in a variety of applications in which reduction of thermal conductivity is important.

See supplementary material for an in-depth description of the modeling of the TDTR data in this study. This includes a discussion of analysis using multiple thermal excitation modulation frequencies in our measurements, analysis of our measured data using variable multilayer configurations, and taking into account potential non-diffusive thermal transport in the substrate of our samples. Additionally, we outline the formulation of the error associated with our measurement.

[1]D. R. Clarke, Surf. Coat. Technol. **163–164**(0), 67–74 (2003).
[2]D. R. Clarke and S. R. Phillpot, Mater. Today **8**(6), 22–29 (2005).
[3]M. Zebarjadi, K. Esfarjani, M. S. Dresselhaus, Z. F. Ren, and G. Chen, Energy Environ. Sci. **5**(1), 5147–5162 (2012).
[4]P. G. Klemens, Proc. Phys. Soc. Sect. A **68**(12), 1113–1128 (1955).
[5]D. G. Cahill and F. Watanabe, Phys. Rev. B **70**(23), 235322 (2004).
[6]D. G. Cahill, F. Watanabe, A. Rockett, and C. B. Vining, Phys. Rev. B-Condens. Matter Mater. Phys. **71**(23), 235202 (2005).
[7]R. Cheaito, J. C. Duda, T. E. Beechem, K. Hattar, J. F. Ihlefeld, D. L. Medlin, M. A. Rodriguez, M. J. Campion, E. S. Piekos, and P. E. Hopkins, Phys. Rev. Lett **109**(19), 195901 (2012).
[8]B. Abeles, Phys. Rev. **131**(5), 1906–1911 (1963).
[9]N. Mingo, D. Hauser, N. P. Kobayashi, M. Plissonnier, and A. Shakouri, Nano Lett. **9**(2), 711–715 (2009).
[10]W. Kim, J. Zide, A. Gossard, D. Klenov, S. Stemmer, A. Shakouri, and A. Majumdar, Phys. Rev. Lett. **96**(4), 45901 (2006).
[11]E. Sachet, C. T. Shelton, J. S. Harris, B. E. Gaddy, D. L. Irving, S. Curtarolo, B. F. Donovan, P. E. Hopkins, P. A. Sharma, A. L. Sharma, J. Ihlefeld, S. Franzen, and J.-P. Maria, Nat. Mater. **14**(4), 414–420 (2015).
[12]J. C. Duda, P. E. Hopkins, Y. Shen, and M. C. Gupta, Phys. Rev. Lett. **110**(1), 015902 (2013).
[13]P. Dongmo, Y. Zhong, P. Attia, C. Bomberger, R. Cheaito, J. F. Ihlefeld, P. E. Hopkins, and J. Zide, 093710, 1–5 (2012).
[14]J. C. Duda, T. S. English, E. S. Piekos, T. E. Beechem, T. W. Kenny, and P. E. Hopkins, J. Appl. Phys. **112**(7), 073519 (2012).
[15]C. S. Gorham, K. Hattar, R. Cheaito, J. C. Duda, J. T. Gaskins, T. E. Beechem, J. F. Ihlefeld, L. B. Biedermann, E. S. Piekos, D. L. Medlin, and P. E. Hopkins, Phys. Rev. B **90**(2), 24301 (2014).
[16]S.-M. Lee, D. G. Cahill, and R. Venkatasubramanian, Appl. Phys. Lett. **70**(22), 2957–2959 (1997).
[17]G. Pernot, M. Stoffel, I. Savic, F. Pezzoli, P. Chen, G. Savelli, A. Jacquot, J. Schumann, U. Denker, I. Mönch, C. Deneke, O. G. Schmidt, J. M. Rampnoux, S. Wang, M. Plissonnier, A. Rastelli, S. Dilhaire, and N. Mingo, Nat. Mater. **9**(6), 491–495 (2010).

[18]Y. S. Touloukian, R. W. Powell, C. Y. Ho, and P. G. Klemens, *Thermophysical properties of matter – the TPRC data series, Volume 2, Thermal conductivity – nonmetallic solids Reannouncement, Data book* (U.S. Department of Energy, 1971), pp. 1–1172.

[19]D. G. Cahill, M. Katiyar, and J. R. Abelson, Phys. Rev. B **50**(9), 6077–6081 (1994).

[20]C. W. Nan, R. Birringer, D. R. Clarke, and H. Gleiter, J. Appl. Phys. **81**(10), 6692–6699 (1997).

[21]W. Kim and A. Majumdar, J. Appl. Phys. **99**(8), 084306 (2006).

[22]A. Minnich and G. Chen, Appl. Phys. Lett. **91**(7), 073105 (2007).

[23]W. B. Daniels, Phys. Rev. Lett. **8**(1), 3–4 (1962).

[24]C. J. Glassbrenner and G. A. Slack, Phys. Rev. **134**(4A), A1058–A1069 (1964).

[25]D. K. Brice, Phys. Rev. **140**(4A), A1211–A1222 (1965).

[26]R. C. Newman, J. Phys. C: Solid State Phys. **18**(30), L967 (1985).

[27]M. Asheghi, Y. K. Leung, S. S. Wong, and K. E. Goodson, Appl. Phys. Lett. **71**(13), 1798 (1997).

[28]E. Pop, S. Sinha, and K. E. Goodson, Proc. IEEE **94**(8), 1587–1601 (2006).

[29]P. E. Hopkins, L. M. Phinney, J. R. Serrano, and T. E. Beechem, Phys. Rev. B **82**(8), 85307 (2010).

[30]A. M. Marconnet, M. Asheghi, and K. E. Goodson, J. Heat Transfer **135**(6), 061601 (2013).

[31]J. R. de Laeter, J. K. Böhlke, P. De Bièvre, H. Hidaka, H. S. Peiser, K. J. R. Rosman, and P. D. P. Taylor, Pure Appl. Chem. **75**(6), 683–800 (2003).

[32]W. B. Pearson, *A Handbook of Lattice Spacings and Structures of Metals and Alloys* (Pergamon Press, New York, 1958), Vol. 1.

[33]J. L. Tallon and A. Wolfenden, J. Phys. Chem. Solids **40**(11), 831–837 (1979).

[34]M. A. Hopcroft, W. D. Nix, and T. W. Kenny, Microelectromech. Syst. J. **19**(2), 229–238 (2010).

[35]D. G. Cahill, S. K. Watson, and R. O. Pohl, Phys. Rev. B **46**(10), 6131–6140 (1992).

[36]J. L. Murray and A. J. McAlister, Bull. Alloy Phase Diagrams **5**(1), 74 (1984).

[37]D. G. Cahill, Rev. Sci. Instrum. **75**(12), 5119–5122 (2004).

[38]P. E. Hopkins, J. R. Serrano, L. M. Phinney, S. P. Kearney, T. W. Grasser, and C. T. Harris, J. Heat Transfer **132**(8), 081302 (2010).

[39]A. J. Schmidt, X. Chen, and G. Chen, Rev. Sci. Instrum. **79**(11), 114902 (2008).

[40]J. Callaway, Phys. Rev. **113**(4), 1046–1051 (1959).

[41]R. Tubino, L. Piseri, and G. Zerbi, J. Chem. Phys. **56**(3), 1022–1039 (1972).

[42]W. Fulkerson, J. P. Moore, R. K. Williams, R. S. Graves, and D. L. McElroy, Phys. Rev. **167**(3), 765–782 (1968).

[43]A. Jain and A. J. H. McGaughey, Phys. Rev. B-Condens. Matter Mater. Phys. **93**(8), 081206(R) (2016).

[44]A. Majumdar and P. Reddy, Appl. Phys. Lett. **84**(23), 4768–4770 (2004).

[45]J. L. Hostetler, A. N. Smith, D. M. Czajkowsky, and P. M. Norris, Appl. Opt. **38**(16), 3614–3620 (1999).

[46]P. Singh, M. Seong, and S. Sinha, Appl. Phys. Lett. **102**(18), 181906 (2013).

[47]H. K. Lyeo and D. G. Cahill, Phys. Rev. B-Condens. Matter Mater. Phys. **73**(14), 144301 (2006).

[48]G. T. Hohensee, R. B. Wilson, and D. G. Cahill, Nat. Commun. **6**, 6578 (2015).

[49]A. Giri, J. T. Gaskins, B. F. Donovan, C. Szwejkowski, R. J. Warzoha, M. A. Rodriguez, J. Ihlefeld, and P. E. Hopkins, J. Appl. Phys. **117**(10), 105105 (2015).